

This document is confidential and is proprietary to the American Chemical Society and its authors. Do not copy or disclose without written permission. If you have received this item in error, notify the sender and delete all copies.

**Na₃V₂(PO₄)₃@Carbon Nanofibers: High Mass Loading
Electrode Approaching Practical Sodium Secondary
Batteries Utilizing Ionic Liquid Electrolytes**

Journal:	<i>ACS Applied Energy Materials</i>
Manuscript ID	ae-2019-00176b.R1
Manuscript Type:	Article
Date Submitted by the Author:	n/a
Complete List of Authors:	Hwang, Jinkwang; Kyoto University , Graduate School of Energy Science Matsumoto, Kazuhiko; Kyoto University , Graduate School of Energy Science Hagiwara, Rika; Kyoto University , Graduate School of Energy Science

SCHOLARONE™
Manuscripts

1
2
3
4 **Na₃V₂(PO₄)₃@Carbon Nanofibers: High Mass Loading Electrode**
5
6
7 **Approaching Practical Sodium Secondary Batteries**
8
9 **Utilizing Ionic Liquid Electrolytes**
10

11 Jinkwang Hwang,^a Kazuhiko Matsumoto,^{*a,b} Rika Hagiwara^{a,b}
12
13
14
15

16 a. Graduate School of Energy Science, Kyoto University, Sakyo-ku, Kyoto 606-8501, Japan
17

18
19 b. Unit of Elements Strategy Initiative for Catalysts & Batteries (ESICB), Kyoto University,
20
21 Katsura, Kyoto 615-8510, Japan
22
23
24
25
26

27 *Corresponding author: Kazuhiko Matsumoto
28
29

30 E-mail: k-matsumoto@energy.kyoto-u.ac.jp
31
32
33
34
35
36
37
38
39
40
41
42
43
44
45
46
47
48
49
50
51
52
53
54
55
56
57
58
59
60

ABSTRACT

Practical sodium secondary batteries require high power, high energy density, and long cyclability. The NASICON-type $\text{Na}_3\text{V}_2(\text{PO}_4)_3$ (NVP) is often investigated as a positive electrode material due to its high operation voltage, structural stability, and high Na^+ ion conductivity. To overcome its low electronic conductivity, NVP requires carbon-coating or the addition of conductive materials for practical use. In this study, carbon nanofibers (CNFs) are incorporated as a conductive material along with glucose for carbon coating and fixing CNF frames to NVP particles. A uniform NVP composite and CNFs network (NVPC@CNFs) are obtained by a combination of sonication and the sol-gel method. Electrochemical measurements using a high mass loading electrode around ~ 8.5 mg-active material cm^{-2} and $\text{Na}[\text{FSA}]-[\text{C}_2\text{C}_1\text{im}][\text{FSA}]$ ($\text{C}_2\text{C}_1\text{im}$ = 1-ethyl-3-methylimidazolium, FSA = bis(fluorosulfonyl)amide) ionic liquid electrolyte suggest safe operations of sodium secondary batteries up to intermediate temperatures ($\sim 373\text{K}$). The rate performance further improved by using the NVPC@CNFs compared to NVPC, exhibit a high rate capability (at high geometric current density) of 51.1 mAh g^{-1} at 10C (10.0 mA cm^{-2}) at 298 K and 82.3 mAh g^{-1} at 100C (100 mA cm^{-2}) at 363 K ($1\text{C} = 118$ mA g^{-1} , 1.00 mA cm^{-2}). Furthermore, this material with an ionic liquid electrolyte exhibits superior Coulombic efficiencies over 3000 cycles of 99.9%. Electrochemical measurements (electrical impedance spectroscopy, charge-discharge test, cycle test, and rate performance test) clarify the electrochemical characteristics of this material.

Keywords: Sodium secondary battery; NASICON; Carbon nanofiber; High mass loading electrode; Ionic liquid

Introduction

Electrical energy is the preferred form of consumer energies due to its high usability. In 2002, 40% of the energy consumed in the United States was in the form of electricity.¹⁻² Consequently, many energy carriers emphasize generating electricity. In an effort to replace a portion of conventional energy generation systems that use fossil fuels, environmentally benign renewable energy sources such as solar and wind have drawn global attention.³⁻⁶ However, energy storage systems (ESSs) are essential to facilitate renewable energy sources due to their intermittent production. For the ESSs proposed to date, those using secondary battery systems are advantageous with respect to their high power and energy densities, pollution-free operations, high efficiency, simple maintenance, and versatility.³⁻⁶ Although lithium secondary batteries exhibit an outstanding performance and dominate the global secondary battery market, the low natural abundance, high cost, and uneven distribution (located primarily in South America) of lithium resources⁷⁻⁸ prevent the distribution of ESSs using lithium secondary batteries.

In contrast, sodium resources are abundant and evenly distributed around the world. Because sodium does not suffer from the aforementioned issues associated with lithium, sodium secondary batteries are feasible for large-scale energy storage applications. Sodium has the second smallest ionic radius of alkaline metals⁹ (1.02 Å for Na⁺ and 0.76 Å for Li⁺ in the case of 6- coordination¹⁰). Thus, the development of high-performance sodium secondary batteries can be expedited using analogous techniques as those for lithium secondary batteries. Electrode materials for sodium secondary batteries have been vigorously studied. For examples, transition metal polyanion compounds¹¹⁻¹⁴ and layered O3- and P2-type transition metal oxides¹⁵⁻¹⁸ exhibit prominent performances among positive electrode materials for sodium secondary batteries.

1
2
3
4 A sodium superionic conductor (NASICON) is a well-known electrode material with
5
6 a transition metal polyanionic structure. Polyanionic compounds typically form a structural
7
8 framework based on the XO_4 ($X = P, S, Si, As, Mo, \text{ or } W$) polyanion unit and MO_x ($M =$
9
10 transition metal) polyhedral unit. The NASICON-type $Na_3V_2(PO_4)_3$ (NVP) possesses an open
11
12 framework that provides facile Na ion transport. This feature leads to its renowned high Na^+
13
14 conductivity.^{6, 19-31}
15
16

17
18
19 NVP acts as both positive and negative electrode materials. The former function is
20
21 derived from the V^{3+}/V^{4+} redox reaction with a theoretical capacity of 117.6 mAh g^{-1} based on
22
23 the two-electron reaction of $Na_3V_2(PO_4)_3 \rightleftharpoons NaV_2(PO_4)_3 + 2Na^+ + 2e^-$, whereas the latter is
24
25 from the V^{3+}/V^{2+} redox reaction with a theoretical capacity of 55 mAh g^{-1} based on the one-
26
27 electron reaction of $Na_4V_2(PO_4)_3 \rightleftharpoons Na_3V_2(PO_4)_3 + Na^+ + e^-$.^{23, 28-30} Although previous studies
28
29 have reported that NVP suffers from a low cyclability and rate capability due to its low
30
31 electronic conductivity,^{19-20, 24-26, 29} new strategies such as carbon coating, introducing
32
33 conductive materials, and morphology control have overcome these obstacles.^{6, 19-31} Our
34
35 previous study on a carbon-coated coral-reef morphology NVP composite (NVPC) using an
36
37 ionic liquid (IL) electrolyte exhibited a superior rate performance with a capacity retention of
38
39 42.2 mAh g^{-1} at 298 K and 94.3 mAh g^{-1} at 363 K both at 20C. Moreover, only a 10.8%
40
41 capacity degradation was observed after 5000 cycles.⁶
42
43
44
45
46

47
48 Organic solvent electrolytes exhibit reliable performances in secondary batteries but
49
50 have safety issues regarding volatility and flammability.³²⁻³⁴ Thus, as the battery size increases,
51
52 so does the risk of significant safety problems.³⁵ On the other hand, ionic liquid electrolytes
53
54 are nonflammable, chemically, electrochemically, and thermally stable.³⁶⁻⁴⁰ This is especially
55
56 important when considering room to intermediate-temperature operations of sodium secondary
57
58 batteries.^{6, 41-42} Although there is a concern that the high viscosity of ionic liquid electrolytes
59
60

1
2
3
4 will degrade the performance compared to organic electrolytes at room temperature,^{32, 43-44} this
5
6 is not always true. Recent reports have revealed that ionic liquid electrolytes outperform
7
8 organic electrolytes in cyclability and rate capability.^{6, 44-45} The former has been attributed to
9
10 the formation of a stable solid-electrolyte interphase (SEI) and electrochemical stability.
11
12
13

14 In this study, we propose a new preparation method of NVPC@CNF (CNF = carbon
15
16 nanofiber). CNFs are great materials for electronic conductive additives to enhance electron
17
18 transfer and to improve the contact efficiency between particles as well as between particles
19
20 and the electrolyte.⁴⁶⁻⁴⁸ Composites are prepared via a combination of sonication and the sol-
21
22 gel method. The electrochemical properties are examined using two different types of
23
24 electrolytes (organic solvent electrolyte and ionic liquid electrolyte). Specifically, the
25
26 electrochemical performances of high mass loading electrodes (~ 8.5 mg-active material cm^{-2})
27
28 are compared between 1M NaPF_6 in PC for an organic solvent electrolyte³² and Na[FSA]-
29
30 $[\text{C}_2\text{C}_1\text{im}][\text{FSA}]$ ($\text{C}_2\text{C}_1\text{im}$ = 1-ethyl-3-methylimidazolium) (Na[FSA] molar fractions 0.4) ionic
31
32 liquid electrolyte⁴⁹ to investigate the importance of the electrode material preparation and the
33
34 performance enhancement utilizing an ionic liquid electrolyte at room to intermediate
35
36 temperatures.
37
38
39
40
41
42
43
44
45
46
47
48
49
50
51
52
53
54
55
56
57
58
59
60

EXPERIMENTAL SECTION

Apparatus and Materials

Volatile materials were handled in a vacuum line constructed using stainless steel, borosilicate glass, and PFA (tetrafluoroethylene-perfluoroalkylvinylether copolymer). Nonvolatile materials were handled under a dry argon atmosphere in a glove box. V_2O_5 (Sigma-Aldrich Chemistry, purity 99.6%), oxalic acid dihydrate (Wako Pure Chemical Industries, purity 99.5–100.2%), NaOH (Wako Pure Chemical Industries, purity 97.0%), $NH_4H_2PO_4$ (Wako Pure Chemical Industries, purity 99.0%), and glucose (Wako Pure Chemical Industries) were used as received.

Preparation procedures of NVPC@CNFs

Powdery NVPC@CNFs samples were prepared via sonication and the sol-gel method (**Figure 1**). The NVP precursor was prepared by dissolving 1.8188 g of V_2O_5 (10.000 mmol) and 6.3035 g of oxalic acid dihydrate (5.0002 mmol) into 20 mL of ion-exchanged water at 353 K by continuously stirring using a magnetic bar. Oxalic acid works as a reducing agent for vanadium reduction. As the mixture turned into a blue homogeneous solution, 1.1991 g of NaOH (29.980 mmol), 3.4507 g of $NH_4H_2PO_4$ (29.998 mmol), and 1.7115 g of glucose (9.500 mmol) were added to the solution and stirred for an additional 3 h. Glucose was used as the carbon source and glue for the CNF frameworks and NVP particles. CNFs (0.5 g, mean diameter of 150 nm) were immersed in ion-exchanged water in a beaker at 353 K and sonicated for 30 min. Then the NVP precursor solution was added to the ion-exchanged water containing the dispersed CNFs. The mixture was vigorously stirred using a stirring magnet bar coated with PTFE (polytetrafluoroethylene) at 353 K and sonicated for 30 min. The water was completely evaporated at 393 K in a day. The resulting residue was calcined at 623 K for 5 h under an Ar flow and successively baked at 1073 K under an Ar flow for 8 h. The NVPC with (carbon

content 10.8wt%) samples used for comparison were prepared as previously reported.⁶

Material Characterization

X-ray diffraction (XRD) patterns were collected in the Bragg-Brentano geometry using a Rigaku SmartLab diffractometer with Ni-filtered Cu- $K\alpha$ radiation (40 kV and 30 mA) and a silicon strip high-speed detector (Rigaku D/teX Ultra 250). Rietveld refinement was performed by the FullProf software.⁵⁰ The crystal structures were visualized using crystallographic data from the Rietveld refinement and the VESTA program.⁵¹ The morphologies of the NVPC@CNFs were observed by scanning electron microscopy (SEM) (Hitachi SU-8020) and energy dispersive X-ray analysis (EDX) (Horiba EMAXEvolution X-max). The surface area of the electrode materials was determined by the BET method⁵² based on the results of nitrogen adsorption analysis by a Tristar II 3020 (Micromeritics). Raman spectra were recorded on a Nanofinder 30 (Tokyo Instruments, Inc.) instrument using the 632.8 nm excitation line of a He-Ne laser. The Raman shift was calibrated by a single-crystal Si. The samples for Raman spectroscopy were loaded in a glass cell in the air.

Electrode and Cell Preparation

Sodium metal (Sigma-Aldrich Chemistry, 99.95% purity) was cut into a disk (16-mm diameter) and fixed on an Al plate current collector as the negative electrode. The positive electrode was prepared by mixing the NVPC@CNFs composite, Super C65, and PVdF (90:5:5 wt%) in *N*-methylpyrrolidone and pasting the mixture onto Al foil. The mass loading of the active material in the electrodes was approximately 8.5 mg-active material cm⁻² after drying. The electrodes with different mass loading were prepared in the same manner as above by changing their thickness. For the symmetric full cell test, mass loadings of 2.0 mg cm⁻² and 4.0 mg cm⁻² for NVPC@CNFs were used for the positive and negative electrodes, respectively. A NVPC electrode was prepared by the NVPC composite, Super C65, and PVdF (80:15:5 wt%). Coin

1
2
3
4 cells (type-2032) were assembled in an argon-filled glove box. The specific contribution of
5
6 NVP in NVPC@CNFs electrode is 74.7wt% and NVPC electrode is 71.4wt%.
7
8

9
10 Na[FSA]-[C₂C₁im][FSA] with a 40:60 molar ratio of ionic liquid and 1 M Na[FSA]-
11
12 PC (propylene carbonate, Kishida Chemical) of organic electrolyte were used as the
13
14 electrolytes. The salts, Na[FSA] (Mitsubishi Materials Electronic Chemicals, purity >99%),
15
16 and [C₂C₁im][FSA] (Kanto Chemical, purity >99.9%), were dried under vacuum for 24 h at
17
18 353 K. The ionic liquid electrolyte was prepared by mixing these two salts at a Na[FSA] molar
19
20 fractions of 0.4. The typical water content of this IL system was below 30 ppm according to
21
22 Karl-Fischer titrations (899 Coulometer, Metrohm). A glass microfiber separator was
23
24 impregnated with an ionic liquid at 333 K under vacuum for 1 d prior to the cell assembly. In
25
26 the case of an organic electrolyte, a separator was impregnated with an electrolyte just before
27
28 assembling coin cells in the glove box.
29
30
31
32

33 **Electrochemical Measurements**

34
35 The electrochemical properties were measured at 298 and 363 K. A current density of 0.1C
36
37 (1C = 117 mA g⁻¹) was applied for the charge/discharge test to examine the basic
38
39 electrochemical behavior. Then various discharge current rates of 0.1C to 200C were used in
40
41 the rate capability tests. For all of the half-cell electrochemical measurements, the cutoff
42
43 voltages were fixed at 2.4 and 3.8 V as the lower and upper limits, respectively. The charge-
44
45 discharge properties, rate capabilities, and cycling performances were evaluated using an
46
47 HJ1001SD8 charge-discharge test device (Hokuto Denko). All the electrochemical
48
49 measurements were performed at least 2 h after the relevant temperature adjustments.
50
51
52
53

54 Cells (2032 coin-type) were prepared for the electrochemical impedance spectra (EIS)
55
56 measurements. The cells were assembled under a dry Ar atmosphere. Details about the
57
58 measurement method and cell preparation are in our previous reports.^{14, 53} Measurements were
59
60

1
2
3
4 performed using a VSP potentiostat (Bio-Logic) at 298 and 363 K over a frequency range from
5
6 1 MHz to 40 mHz with a perturbation amplitude of 10 mV.
7
8
9
10
11
12
13
14
15
16
17
18
19
20
21
22
23
24
25
26
27
28
29
30
31
32
33
34
35
36
37
38
39
40
41
42
43
44
45
46
47
48
49
50
51
52
53
54
55
56
57
58
59
60

RESULT AND DISCUSSION

Figure 1 schematically illustrates the preparation of NVPC@CNFs via a combination of sonication and the sol-gel method. The CNFs are well-dispersed by sonication in ion-exchanged water at 353 K, and mixing of the dispersed CNFs with the precursor of NVPC provides CNFs embedded in the pure NVP phase.

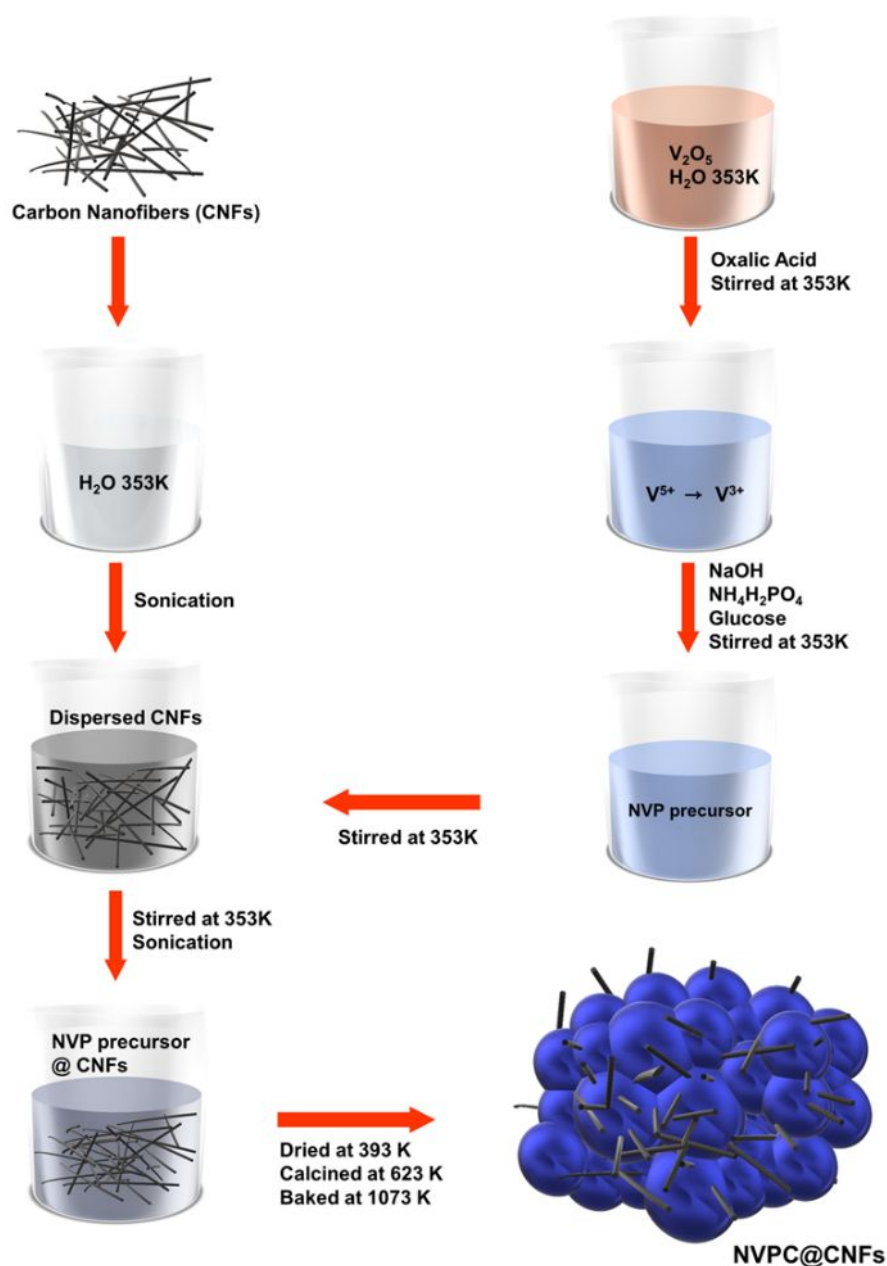
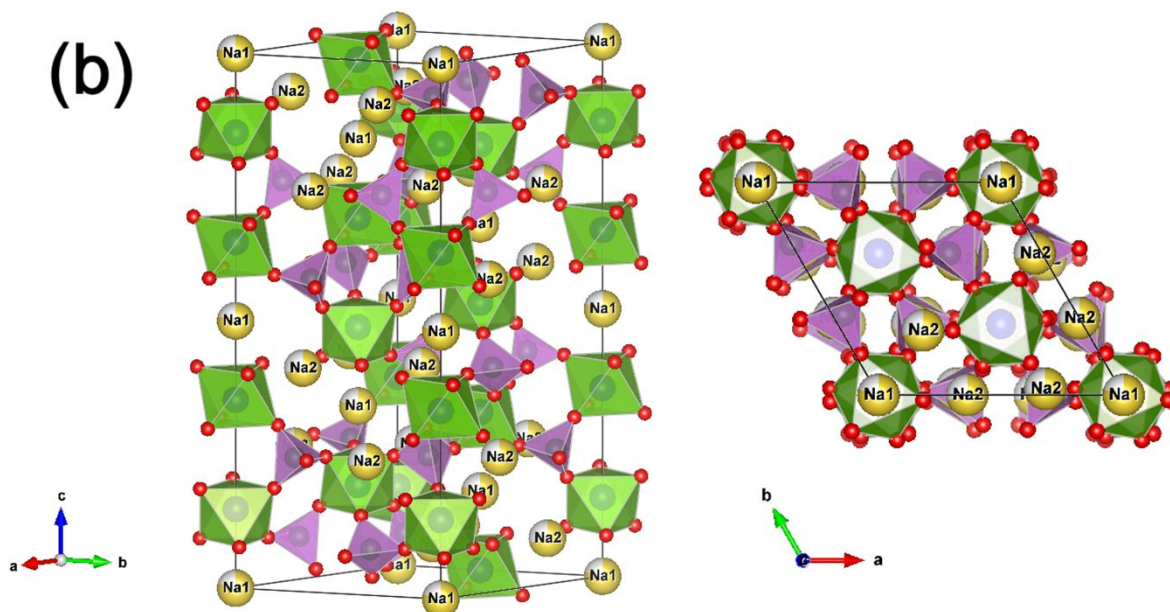
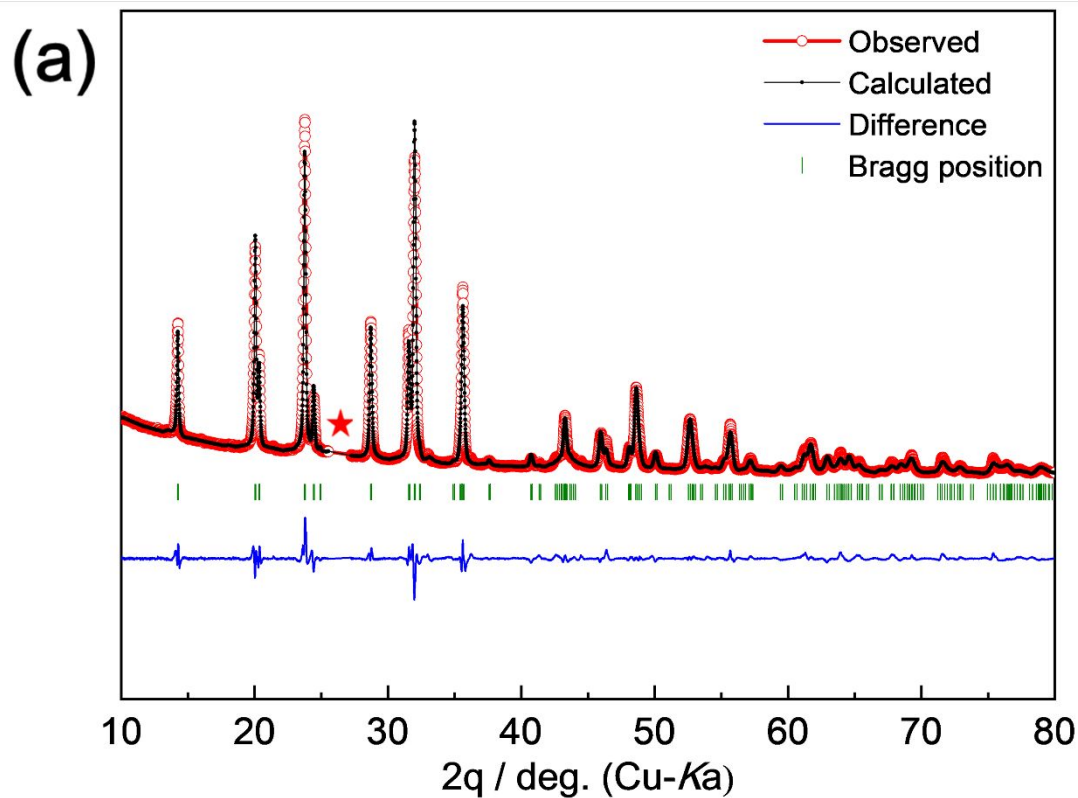


Figure 1. Schematic illustration of the preparation of NVPC@CNFs.

Figure 2 shows the XRD patterns of the prepared NVPC@CNFs composites. All of the peaks except for the one at 26.4° are indexed as the rhombohedral lattice system, and can be fitted with a pure NVP phase under the $R\bar{3}c$ space group via the Rietveld refinement (**Table 1**). The peak at 26.4° is assigned to CNFs (Figure S1 in the Supporting Information). The lattice parameters of NVP are $a = 8.7294(1)$ and $c = 21.8590(4)$ Å ($R_{wp} = 13.2\%$), which agree with the crystallographic data in previous works.^{6, 22, 24, 54-55} These crystallographic data confirm that NVP is a pure phase without impurities and CNFs do not influence the NVP crystal structure. The refined crystal structural model in Figure 2 (b) contains corner-sharing with octahedral VO₆ and tetrahedral PO₄, forming an open framework of the V₂(PO₄)₃ units along the *c*-axis for Na ion diffusion. The constituent Na ions selectively occupy two distinct sites labeled as Na1 (occupancy of 0.781) and Na2 (occupancy of 0.727). However, a heating temperature of 1073 K is necessary to obtain the pure NVP phase; NVPC@CNFs heated at 873 K is mainly composed of amorphous NVPC@CNFs precursor according to the XRD result (Figure S1), though a small amount of the NVP phase is confirmed.

Table 1. Crystallographic data of the NVP phase in NVPC@CNFs by Rietveld refinement

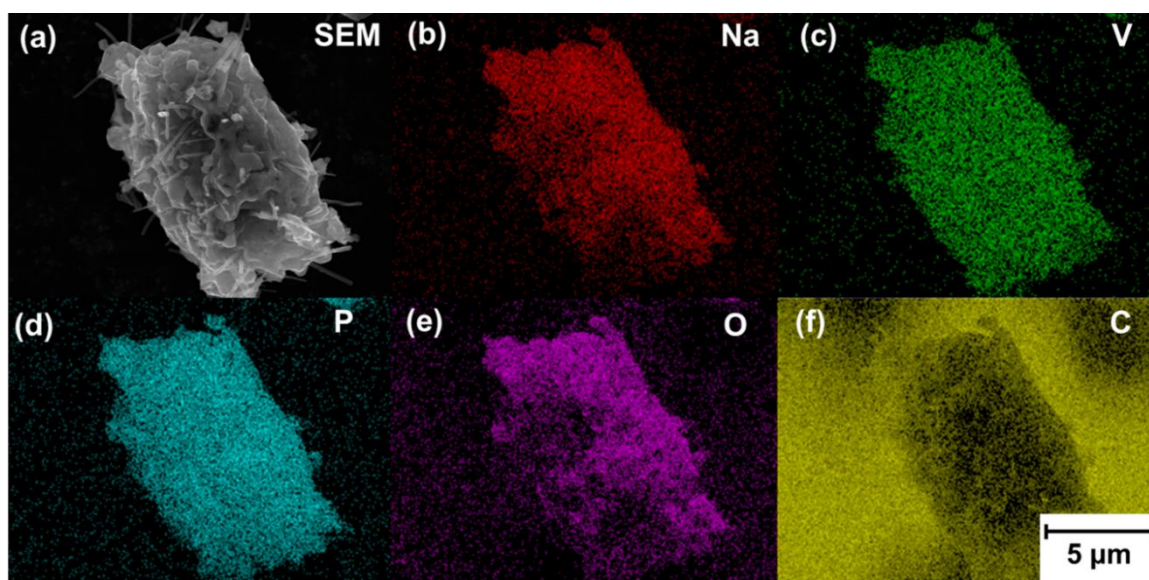
Refinement results for the NVP phase in NVPC@CNFs (S.G. $R\bar{3}c$)						
$R_p = 12.8\%$, $R_{wp} = 13.2\%$, $R_e = 2.53\%$, $a = 8.7302(2)$ Å, $c = 21.8592(2)$ Å						
Wyckoff						
Atom	symbol	<i>x</i>	<i>y</i>	<i>z</i>	$B_{iso}/\text{Å}^2$	Occup.
Na1	6b	0	0	0	0.5	0.781(2)
Na2	18e	0.6375(4)	0	0.2500	0.5	0.727(6)
V	12c	0	0	0.1477(5)	0.5	1.000
P	18e	0.2889(2)	0	0.2500	0.5	1.000
O1	36f	0.1814(3)	0.9696(3)	0.1926(9)	0.5	1.000
O2	36f	0.1932(3)	0.1698(3)	0.0883(1)	0.5	1.000



50
51
52
53
54
55
56
57
58
59
60

Figure 2. (a) Rietveld refinement results of NVPC@CNFs. Red star indicates the removed region from the patterns to avoid the strong peak of CNFs in the refinement. See Table 1 for the crystallographic data of the NVPC@CNFs and Fig. S2 in the Supporting Information for the full XRD patterns. (b) The refined NVP structural model, yellow, red, green and purple denote sodium, oxygen, VO₆, and PO, respectively.

1
2
3
4
5
6
7 **Figure 3** shows the morphology of NVPC@CNFs observed by SEM with the EDX
8 mapping results. The SEM image of NVPC@CNFs shows that CNFs and additional carbon by
9 thermal decomposition of glucose form an electronically conductive path at the surface and
10 inside the NVP particles. The high magnification SEM images confirm a uniform CNF
11 distribution onto the NVPC@CNFs composite (Figure S2). The EDX (Na, V, P, and O)
12 results suggest that all the elements are evenly distributed onto the NVPC@CNFs composite. These
13 results agree reasonably well with the theoretical composition. (See Figure 3 caption for the
14 observed and theoretical compositions.) In the case of carbon, the EDX image detects strong
15 peaks corresponding to the carbon tape. Combustion elemental analysis reveals that the amount
16 of carbon content is 17.0%.



47 **Figure 3.** (a) SEM image and (b-f) EDX mappings of the elements in the NVPC@CNFs sample.
48 EDX Obs: Na, 15.1; V, 22.4; P, 20.4; O, 42.1 (wt%), Calc. for NVP: Na, 13.9; V, 23.0; P, 20.4;
49 O, 42.7 (wt%). Carbon content (17.0 wt% by combustion analysis, including 6.2 wt%
50 contribution of CNFs) is excluded.

51
52
53 **Figure 4** shows the Raman spectra of two different carbon in NVPC@CNFs (carbon
54 coating and CNF incorporation) and NVPC (carbon coating). The peaks at 1360 and 1580 cm^{-1}
55 correspond to the D-band and G-band, which represent the disordered graphene and ordered
56
57
58
59
60

graphene structures in NVPC@CNFs and NVPC.⁵⁶ The peak at 2684 cm^{-1} is the called 2D-band or G'-band, suggesting the existence of CNFs.⁵⁷⁻⁵⁸ The D-band is stronger than the G-band in the NVPC spectrum, indicating that the dominant carbon phase is disordered amorphous graphene. On the other hand, NVPC@CNFs exhibit a stronger G-band than a D-band. This corresponds to the addition of graphitized CNFs. The results of SEM, EDX, XRD, and Raman spectroscopy suggest that this novel method enables a uniform composite of CNFs and a carbon-coated pure NVP phase to be formed. The surface area of NVPC@CNFs was measured by the N_2 adsorption isotherm at 77 K. NVPC@CNFs have a Brunauer-Emmett-Teller (BET) surface area of $6.1\text{ m}^2\text{ g}^{-1}$, which is similar to that of NVPC ($7.7\text{ m}^2\text{ g}^{-1}$). (Figure S3 plots the N_2 adsorption isotherm at 77 K and the BET surface area plot for NVPC@CNFs⁶)

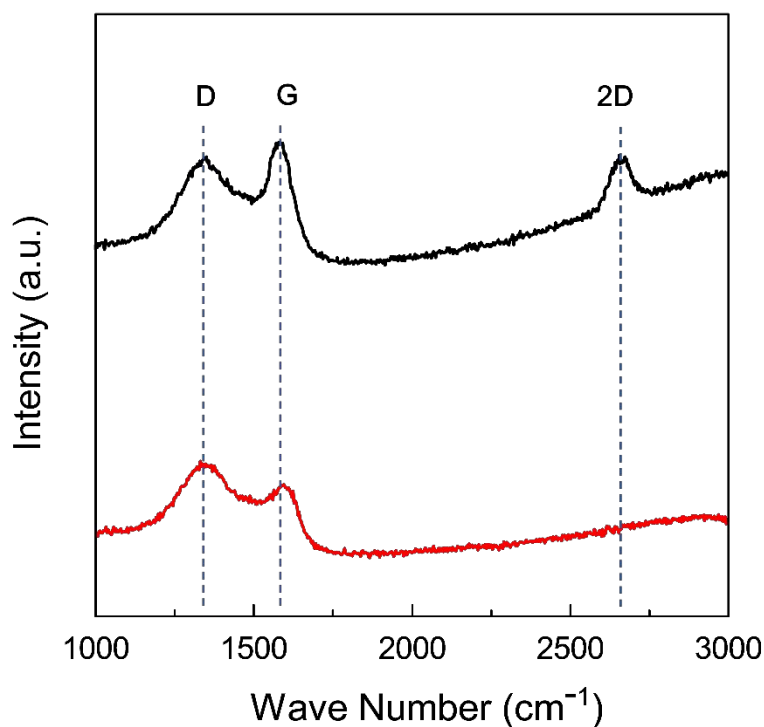


Figure 4. Raman spectra of (a) NVPC@CNFs and (b) NVPC. Symbols G and D denote the G-band originating from the ordered graphene structure and the D-band originating from the structural disorder in the graphene sheet, respectively.

Figure 5 shows the galvanostatic charge-discharge profiles and cycling properties of the Na/IL/NVPC@CNFs cell at 298 K and a current rate of 0.1C (a) and 2C (b). The charging profiles of the first cycle differ from the other cycles. The first charge curve shows a capacity of 116 mAh g⁻¹, which contains some irreversible capacity. All other subsequent cycles are highly stable and exhibit a reversible capacity of 105 mAh g⁻¹ based on the two-electron desodiation/sodiation reaction accompanying the V⁴⁺/V³⁺ redox activity. The flat plateaus at approximately 3.4 V in Figure 5a correspond to the Na₃V₂(PO₄)₃/NaV₂(PO₄)₃ two-phase process.⁶ NVPC@CNFs exhibit a stable cyclability over 200 cycles (Figure 5b). The average Coulombic efficiency during 200 cycles is over 99.9%, and 100.9% of the capacity in the first cycle is retained.

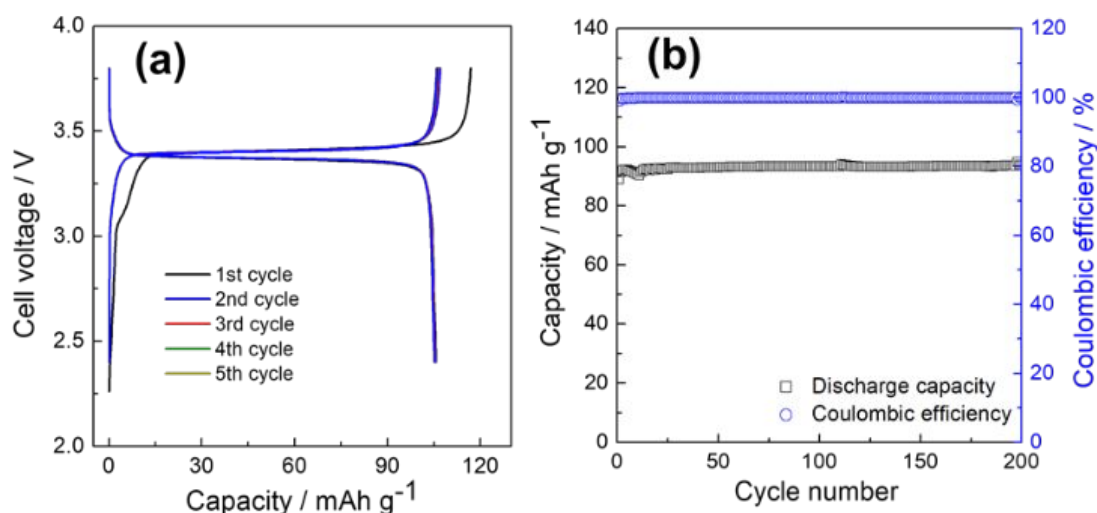


Figure 5. (a) Charge-discharge curves and (b) cycling properties of the Na/IL/NVPC@CNFs cell at 298 K. Current densities: (a) 0.1C and (b) 2C. Cutoff voltages: 2.4–3.8 V. Mass loading: 8.5 mg-active material cm⁻².

To determine the performance at intermediate temperature operations, a cycle test was carried out at 363 K. The cell exhibits a highly stable cycle performance over 200 cycles at 363 K. The reversible capacity is 99.6 mAh g⁻¹ at 2C with an average Coulombic efficiency of 99.1% (Figure S4). These results imply that sodium secondary batteries with an IL electrolyte are free from flammability safety hazards and utilize waste heat to enhance performance, as proposed

1
2
3
4 in previous works.^{6, 59}
5
6

7 Many recent studies have reported that NVP can show a high rate capability by improving the
8 electronic conductivity originating from the phosphate group with the aid of carbon coating,
9 morphology control, or metal ion doping.^{6, 21, 24-25, 27, 54, 60-64} However, mass loading, which
10 significantly affects the rate performance results, is often neglected in rate capability tests. This
11 is because mass loading is directly related to the geometric current density. Prior to the rate
12 capability measurements of NVPC@CNFs, that of NVPC was tested at three different mass
13 loadings: 1.5, 3.0, and 6.0 mg-active material cm⁻² at 298 K and 363 K (Figure S5). NVPC
14 exhibits a high rate capability when the mass loading is small (1.5 mg-active material cm⁻²;
15 capacity retentions of 79.4% at 298 K, and 92.5% at 363 K at 40C). However, this high rate
16 capability decreases as the mass loading increases because the Na ion diffusion paths are
17 prolonged in the composite electrode as the mass loading increases, and is severe at room
18 temperature (capacity retentions of 79.4%, 18.3%, and 0.6% with 1.5, 3.0, and 6.0 mg-active
19 material cm⁻², respectively at 298 K at 40C). On the other hand, the rate capability is
20 maintained at a high level at an intermediate temperature (~363 K) even for a high mass load
21 (capacity retentions comparing at 0.1C to at 40 C of NVP 1.7 mg cm⁻², 3.0 mg cm⁻², and 6.0
22 mg cm⁻² at 363 K are 92.5, 89.5, 86.6%, respectively). Furthermore, at both temperature, there
23 is strong trend that the rate capability is limited by geometric current density. For example, the
24 capacity retention of 3.0 mg cm⁻² at 10C and 6.0 mg cm⁻² at 5C at have the same geometric
25 current density of 3.53 mA cm⁻² exhibit similar capacity retention of 68.3% and 63.2%,
26 respectively at 298 K and 96.1% and 97.3% at 363 K, respectively. The geometric current
27 densities and details on capacity retention are provided in Table S2 and S3 in the supporting
28 information.
29
30
31
32
33
34
35
36
37
38
39
40
41
42
43
44
45
46
47
48
49
50
51
52
53
54
55
56
57
58
59
60

CNF embedding improves the high rate performance of NVPC. **Figures 6a and 7a**

1
2
3
4 show the rate performance test results for NVPC@CNFs using the IL electrolyte. For
5
6 comparison, Figure S6 shows the test with the organic electrolyte of 1M NaPF₆-PC at 298 K
7
8 under the same conditions. NVPC@CNFs exhibit a high rate capability at 298 K regardless of
9
10 the type of electrolyte. NVPC@CNFs using IL electrolyte display 87.5 and 51.0 mAh g⁻¹ at 5
11
12 and 10C, respectively. Moreover, it has a higher mass loading of 8.5 mg-active material cm⁻²
13
14 than that of NVPC with 6.0 mg-active material cm⁻² (c.f. 63.2 and 32.6 mAh g⁻¹ at 5 and 10C,
15
16 respectively). The capacity of the cells after the rate capability test is promptly recovered at a
17
18 low current density of 0.1C, suggesting negligible damage during the rate capability test. In the
19
20 case of NVPC@CNFs using an organic electrolyte, the cell is stabilized after the fifth cycle
21
22 (cf. the cell using IL electrolyte is stable from the first cycle). It exhibits 79.7 and 65.5 mAh
23
24 g⁻¹ at 5 and 10C, respectively. These results indicate that ILs are more favorable to form good
25
26 a passivation layer, and that a well-prepared positive material combined with an IL electrolyte
27
28 shows almost the same electrochemical performance as those using an organic electrolyte.
29
30 Despite concerns about the limited performance of IL at room temperature operations,
31
32 NVPC@CNFs in IL electrolytes show a higher stability with an extremely high Coulombic
33
34 efficiency.
35
36
37
38
39
40
41
42
43
44
45
46
47
48
49
50
51
52
53
54
55
56
57
58
59
60

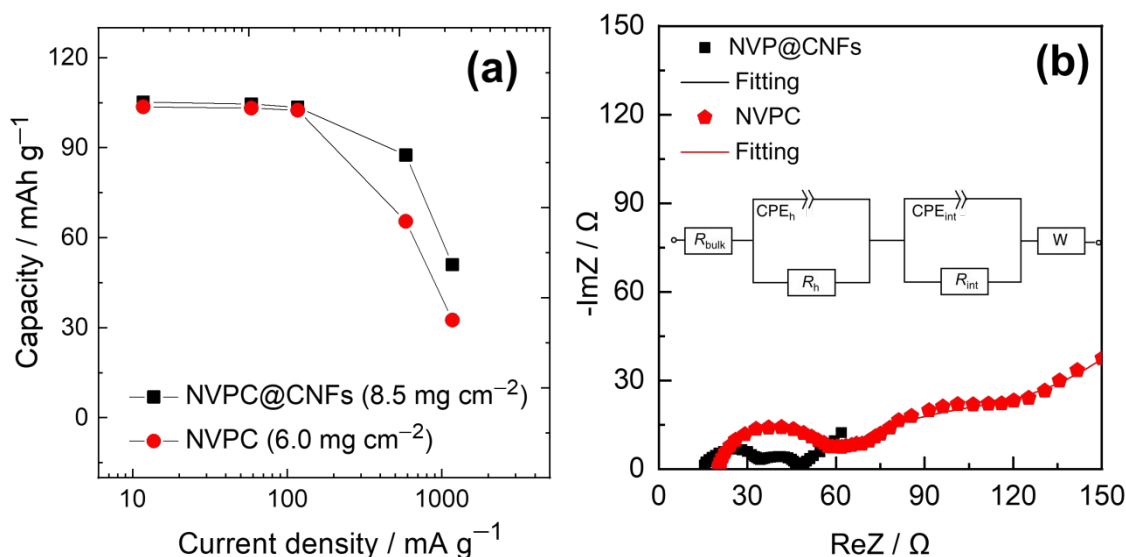


Figure 6. (a) Comparative rate capability plots for Na/NVPC and Na/NVPC@CNFs at 298 K. Current densities: 0.1C for charge and 0.1C to 10C for discharge with cutoff voltages of 2.4–3.8 V. (b) NVPC@CNFs/IL/NVPC@CNFs and NVPC/IL/NVPC symmetric cell EIS. Inset shows an equivalent circuit, where CPE denotes the constant phase element and W denotes the Warburg element at 298 K. SOC= 50%, frequency range: 40 mHz – 100 kHz, ac amplitude: 10 mV. Mass loading: 8.5 and 6.0 mg-active material cm^{-2} for NVPC@CNFs and NVPC, respectively. See Table S1 in Supporting Information for the fitting parameters of the impedance spectra. Characteristic frequencies: R_h : ~ 5000 Hz and R_{int} : ~ 10 Hz. See Tables S2 and S3 in Supporting Information for details about the capacity, capacity retention, and geometric current density.

Symmetric cell EIS is a powerful method to investigate only the targeted electrode.⁵³

⁶⁵⁻⁶⁷ Two identical electrodes at the same state-of-charge were used for the EIS measurement, and the EIS spectra are fitted based on an equivalent circuit (Figure 6b, inset). Figure 6b, which compares symmetric cell EIS of NVPC@CNFs/IL/NVPC@CNFs and NVPC/IL/NVPC (state of charge (SOC) = 50% in both cases), confirms this improvement. Table S1 shows the fitted data. There are two semi-circles with characteristic frequencies of ~ 5000 Hz (high-frequency region denoted as R_h) and ~ 10 Hz (interfacial resistance denoted as R_{int}). R_h is often referred to as the resistance of SEI. A detailed interpretation of this resistance is still difficult, but our recent study revealed that it is strongly influenced by temperature, electrical conductivity of an electrode, surface area, electrolyte concentration, etc., and it is intimately related to electrode

1
2
3
4 performance.⁵³ R_h decreases by half by introducing CNFs into the NVP particles (34.5 Ω for
5 NVPC and 13.7 Ω for NVPC@CNFs). R_{int} refers to the charge-transfer resistance at the
6 electrode-electrolyte interface. The semicircle for NVPC@CNFs corresponds to R_{int} of 18.6 Ω ,
7 which is roughly one-fourth that of NVPC (71.3 Ω) (Table S1).
8
9
10
11
12
13

14 The results suggest that embedded CNFs in NVPC particles improve the electronic
15 conduction between NVP particles and the electrochemical process at the electrode/electrolyte
16 interface.⁶⁸⁻⁷⁰ This facilitates the insertion/desertion of Na^+ ions into the NVP framework and
17 directly improves the rate capability. Since introducing CNFs enhances the rate capability at
18 298 K, the rate capability was further tested at 363 K. Despite a high mass loading of 8.5 mg-
19 active material cm^{-2} , very stable cycles and high discharge capacities of 102.5 mAh g^{-1} at 10C,
20 82.3 mAh g^{-1} at 100C, and 71.7 mAh g^{-1} at 200C are observed (Figure 7c,d).
21
22
23
24
25
26
27
28
29
30
31
32
33
34
35
36
37
38
39
40
41
42
43
44
45
46
47
48
49
50
51
52
53
54
55
56
57
58
59
60

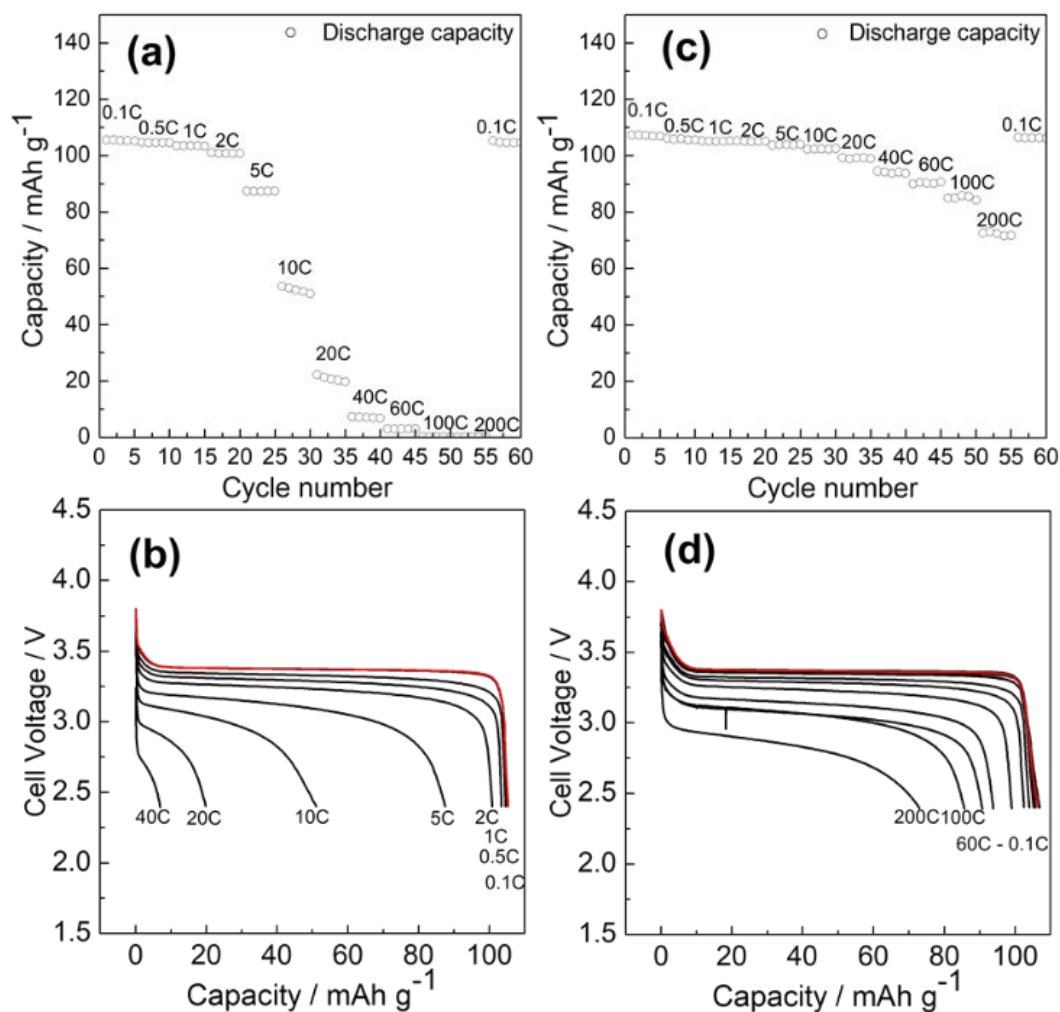
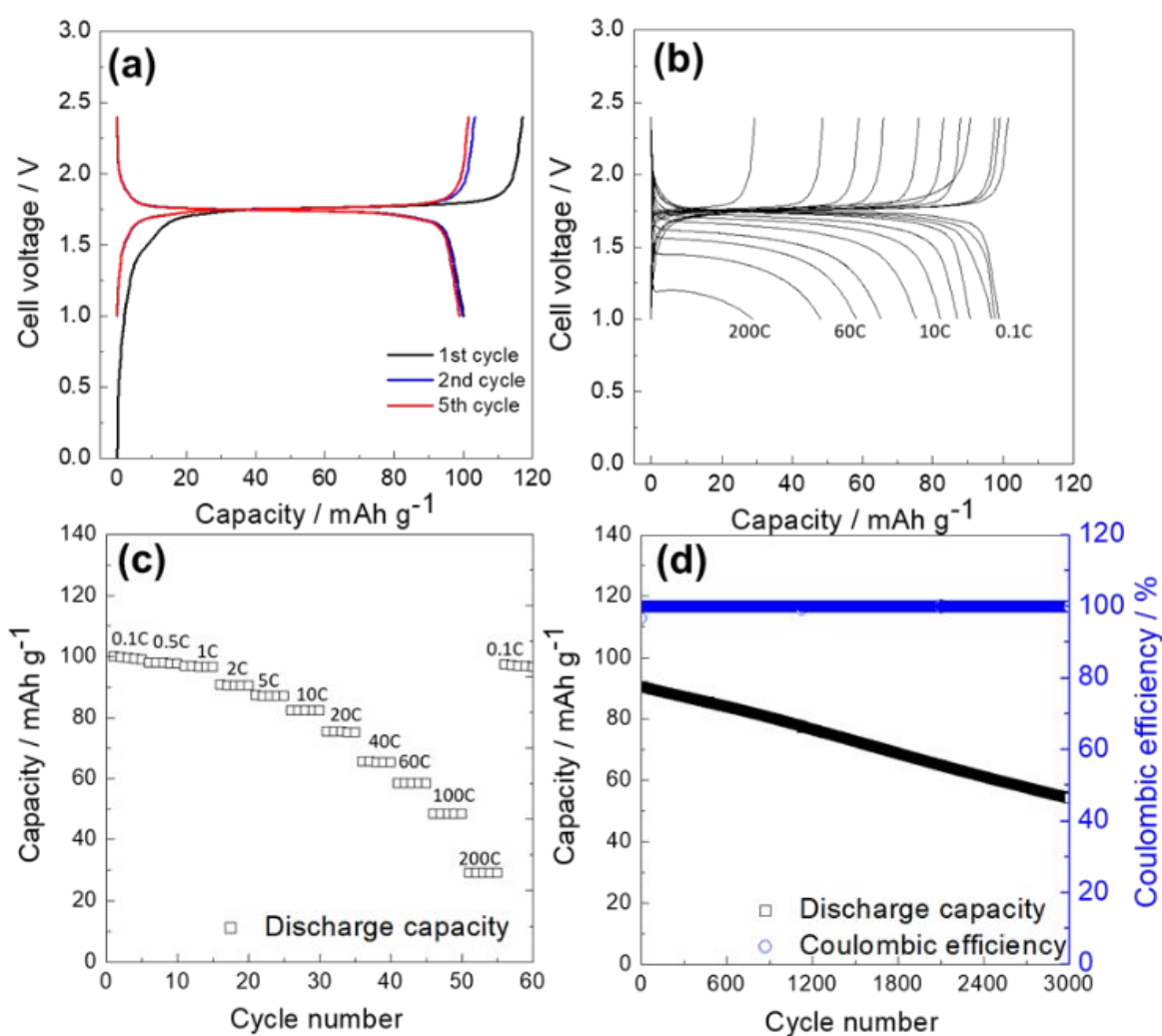


Figure. 7 Rate capabilities of Na/IL/NVPC@CNFs cells at (a, b) 298 K and (c, d) 363 K. Red curves refer to the discharge profile at 0.1C after the rate capability test up to 200C. Current densities: 0.1C for charge and 0.1C–200C for a cycle test with cutoff voltages of 2.4 V–3.8 V. Mass loading: 8.5 mg-active material cm⁻². See Table S2-4, Supporting Information, for details about the capacity, capacity retention and geometric current density.

A symmetric full cell was assembled using two NVPC@CNFs electrodes. The operations of an NVP symmetric full cell is associated with the V³⁺/V⁴⁺ and V²⁺/V³⁺ redox activities for positive and negative electrodes, respectively (See Figure S7 for the V²⁺/V³⁺ redox activity of NVPC@CNFs as a negative electrode). A symmetric full cell can be facilely charged-discharged free from the large polarization of the Na metal counter electrode. The cell exhibits a highly reversible capacity of 99.7 mAh g⁻¹ with an average operation potential of 1.7 V in Figure 8a at 0.1C and 298 K using the IL electrolyte. Outstanding rate capabilities of 82.2

1
2
3
4 mAh g⁻¹ at 10C, 65.4 mAh g⁻¹ at 40C, and 48.3 mAh g⁻¹ at 100C are obtained at 298 K.
5
6
7 Additionally, a superior cycle performance occurs at 2C over 3000 cycles. It delivers a
8
9 reversible capacity of 90.0 mAh g⁻¹ at 2C in the initial cycle and achieves a capacity retention
10
11 of 99.2%, 88.0%, 80.7%, 73.4%, 66.5%, and 60.1 after 100, 1000, 1500, 2000, 2500, and 3000
12
13 cycles, respectively, with the average Coulombic efficiency over 99.9% (Figure 8d). These
14
15 results indicate that NVPC@CNFs prepared by our novel method are simple and feasible for
16
17 building safe and practical sodium secondary batteries.
18
19



20
21
22
23
24
25
26
27
28
29
30
31
32
33
34
35
36
37
38
39
40
41
42
43
44
45
46
47
48
49
50
51
52
53 **Figure 8.** NVPC@CNFs/IL/NVPC@CNFs symmetric full cell electrochemical measurements
54 at 298 K (a) charge-discharge curve, (b, c) rate capability and cycle test, and (d) cycle test.
55 Current densities: 0.1C for charge-discharge test and charge for rate test, 0.1C to 200C for
56 discharge for rate test and 2C for cycle test with cutoff voltages of 1.0–2.4 V
57
58
59
60

CONCLUSIONS

$\text{Na}_3\text{V}_2(\text{PO}_4)_3$ is a promising electrode material for sodium secondary batteries in terms of its high power and energy density. However, an efficient carbon coating and fabrication method is necessary to fabricate materials that maintain high power and energy density while simultaneously achieving a high rate performance. In this study, NVPC@CNFs composites are prepared by a combination of facile sonication and a sol-gel process. This simple method provides CNFs uniformly embedded inside NVPC particles.

With respect to practical applications, electrochemical tests with a high mass loading of $8.5 \text{ mg-active material cm}^{-2}$ were conducted. They also exhibit a stable yet reversible charge-discharge performance and excellent cyclability across a temperature range of 298 K to 363 K. Furthermore, superior rate capabilities of 51.1 mAh g^{-1} at 10C at 298 K and 82.3 mAh g^{-1} at 100C at 363K are achieved. These improvements originate from the unique matrix structure of NVPC@CNFs because this network serves as an electron conductor between particles and facilitates the charge-transfer process on the electrode/electrolyte interface.

In summary, our study demonstrates that for the true rate performance geometric current density have to be considered, and the present simple method efficiently improves the intrinsic electrochemical performance of NVPC@CNFs in the high mass loading electrode material comparing to NVPC. NVPC@CNFs and IL electrolyte are electrochemically, chemically, and thermodynamically stable. Consequently, they are feasible for future battery materials. We expect this study will contribute to the realization of practical sodium secondary batteries. To this end, further studies using full cells as 18650 size batteries or pouch cells should be conducted.

ASSOCIATED CONTENT

Supporting Information

The Supporting Information is available free of charge on the ACS Publications website at DOI:
XXXXXXX.

Electrochemical measurement data (Charge-discharge performance, rate capability and cyclability), electrochemical impedance spectroscopic data (fitting parameters) and analytical data (N₂ adsorption, and BET surface area plots, SEM, and XRD) for electrode materials (PDF)

AUTHOR INFORMATION

Corresponding Author

*Phone: +81 75 753 5827. Fax: +81 75 753 5906. E-mail: k-matsumoto@energy.kyoto-u.ac.jp
(K.M.).

ORCID

Kazuhiko Matsumoto: 0000-0002-0770-9210

Jinkwang Hwang: 0000-0003-4800-3158

Notes

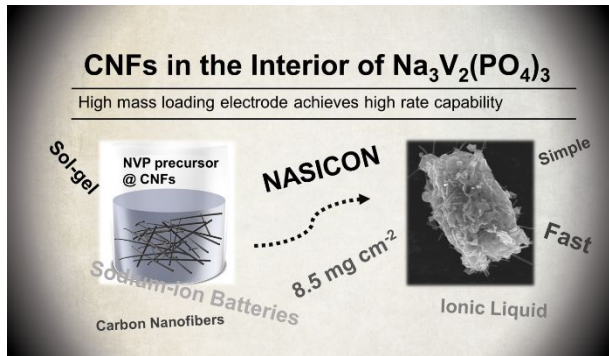
The authors declare no competing financial interest.

ACKNOWLEDGMENT

This study was partly supported by the Advanced Low Carbon Technology Research and

1
2
3
4 Development Program (ALCA) of the Japan Science and Technology Agency (JST) and the
5
6 Japanese Ministry of Education, Culture, Sports, Science and Technology (MEXT) program
7
8
9 “Elements Strategy Initiative to Form Core Research Center.”
10
11
12
13
14
15
16
17
18
19
20
21
22
23
24
25
26
27
28
29
30
31
32
33
34
35
36
37
38
39
40
41
42
43
44
45
46
47
48
49
50
51
52
53
54
55
56
57
58
59
60

TOC Graphic



1
2
3
4
5
6
7
8
9
10
11
12
13
14
15
16
17
18
19
20
21
22
23
24
25
26
27
28
29
30
31
32
33
34
35
36
37
38
39
40
41
42
43
44
45
46
47
48
49
50
51
52
53
54
55
56
57
58
59
60

REFERENCES

- (1) Lin, X.; Salari, M.; Arava, L. M.; Ajayan, P. M.; Grinstaff, M. W. High temperature electrical energy storage: advances, challenges, and frontiers. *Chem. Soc. Rev.* **2016**, *45*, 5848-5887.
- (2) Yang, Z.; Zhang, J.; Kintner-Meyer, M. C.; Lu, X.; Choi, D.; Lemmon, J. P.; Liu, J. Electrochemical energy storage for green grid. *Chem. Rev.* **2011**, *111*, 3577-613.
- (3) Soloveichik, G. L. Battery technologies for large-scale stationary energy storage. *Annu. Rev. Chem. Biomol. Eng.* **2011**, *2*, 503-27.
- (4) Goodenough, J. B.; Park, K. S. The Li-ion rechargeable battery: a perspective. *J. Am. Chem. Soc.* **2013**, *135*, 1167-76.
- (5) Chen, L.; Fiore, M.; Wang, J. E.; Ruffo, R.; Kim, D.-K.; Longoni, G. Readiness Level of Sodium-Ion Battery Technology: A Materials Review. *Adv. Sustainable Syst.* **2018**, *2*, 1700153.
- (6) Hwang, J.; Matsumoto, K.; Hagiwara, R. Na₃V₂(PO₄)₃/C Positive Electrodes with High Energy and Power Densities for Sodium Secondary Batteries with Ionic Liquid Electrolytes That Operate across Wide Temperature Ranges. *Adv. Sustainable Syst.* **2018**, *2*, 1700171.
- (7) Tarascon, J.-M. Is lithium the new gold? *Nat. Chem.* **2010**, *2*, 510.
- (8) Kim, S.-W.; Seo, D.-H.; Ma, X.; Ceder, G.; Kang, K. Electrode Materials for Rechargeable Sodium-Ion Batteries: Potential Alternatives to Current Lithium-Ion Batteries. *Adv. Energy Mater.* **2012**, *2*, 710-721.
- (9) Yabuuchi, N.; Kubota, K.; Dahbi, M.; Komaba, S. Research Development on Sodium-Ion Batteries. *Chem. Rev.* **2014**, *114*, 11636-11682.
- (10) Shannon, R. Revised effective ionic radii and systematic studies of interatomic distances in halides and chalcogenides. *Acta Cryst. A* **1976**, *32*, 751-767.
- (11) Fang, Y.; Liu, Q.; Xiao, L.; Ai, X.; Yang, H.; Cao, Y. High-Performance Olivine NaFePO₄

1
2
3
4
5
6
7
8
9
10
11
12
13
14
15
16
17
18
19
20
21
22
23
24
25
26
27
28
29
30
31
32
33
34
35
36
37
38
39
40
41
42
43
44
45
46
47
48
49
50
51
52
53
54
55
56
57
58
59
60

Microsphere Cathode Synthesized by Aqueous Electrochemical Displacement Method for Sodium Ion Batteries. *ACS Appl. Mater. Interfaces* **2015**, *7*, 17977-17984.

(12) Ellis, B. L.; Makahnouk, W. R.; Makimura, Y.; Toghill, K.; Nazar, L. F. A multifunctional 3.5 V iron-based phosphate cathode for rechargeable batteries. *Nat. Mater.* **2007**, *6*, 749-53.

(13) Kawabe, Y.; Yabuuchi, N.; Kajiyama, M.; Fukuhara, N.; Inamasu, T.; Okuyama, R.; Nakai, I.; Komaba, S. Synthesis and electrode performance of carbon coated Na₂FePO₄F for rechargeable Na batteries. *Electrochem. Commun.* **2011**, *13*, 1225-1228.

(14) Hwang, J.; Matsumoto, K.; Orikasa, Y.; Katayama, M.; Inada, Y.; Nohira, T.; Hagiwara, R. Crystalline maricite NaFePO₄ as a positive electrode material for sodium secondary batteries operating at intermediate temperature. *J. Power Sources* **2018**, *377*, 80-86.

(15) Yabuuchi, N.; Kajiyama, M.; Iwatate, J.; Nishikawa, H.; Hitomi, S.; Okuyama, R.; Usui, R.; Yamada, Y.; Komaba, S. P2-type Na_x[Fe_{1/2}Mn_{1/2}]O₂ made from earth-abundant elements for rechargeable Na batteries. *Nat. Mater.* **2012**, *11*, 512.

(16) Kalluri, S.; Seng, K. H.; Pang, W. K.; Guo, Z.; Chen, Z.; Liu, H. K.; Dou, S. X. Electrospun P2-type Na_{2/3}(Fe_{1/2}Mn_{1/2})O₂ hierarchical nanofibers as cathode material for sodium-ion batteries. *ACS Appl. Mater. Interfaces* **2014**, *6*, 8953-8.

(17) Kwon, M. S.; Lim, S. G.; Park, Y.; Lee, S. M.; Chung, K. Y.; Shin, T. J.; Lee, K. T. P2 Orthorhombic Na_{0.7}[Mn_{1-x}Li_x]O_{2+y} as Cathode Materials for Na-Ion Batteries. *ACS Appl. Mater. Interfaces* **2017**, *9*, 14758-14768.

(18) Guo, S.; Liu, P.; Yu, H.; Zhu, Y.; Chen, M.; Ishida, M.; Zhou, H. A layered P2- and O3-type composite as a high-energy cathode for rechargeable sodium-ion batteries. *Angew. Chem.* **2015**, *54*, 5894-9.

(19) Lim, S. Y.; Kim, H.; Shakoor, R. A.; Jung, Y.; Choi, J. W. Electrochemical and Thermal Properties of NASICON Structured Na₃V₂(PO₄)₃ as a Sodium Rechargeable Battery Cathode:

1
2
3
4 A Combined Experimental and Theoretical Study. *J. Electrochem. Soc.* **2012**, *159*, A1393-
5
6 A1397.

7
8
9 (20) Jian, Z.; Hu, Y. S.; Ji, X.; Chen, W. NASICON-Structured Materials for Energy Storage.
10
11 *Adv. Mater.* **2017**, *29*, 1601925.

12
13 (21) Jian, Z. L.; Zhao, L.; Pan, H. L.; Hu, Y. S.; Li, H.; Chen, W.; Chen, L. Q. Carbon coated
14
15 $\text{Na}_3\text{V}_2(\text{PO}_4)_3$ as novel electrode material for sodium ion batteries. *Electrochem. Commun.*
16
17 **2012**, *14*, 86-89.

18
19 (22) Chotard, J.-N.; Rouse, G.; David, R.; Mentré, O.; Courty, M.; Masquelier, C. Discovery
20
21 of a Sodium-Ordered Form of $\text{Na}_3\text{V}_2(\text{PO}_4)_3$ below Ambient Temperature. *Chem. Mater.* **2015**,
22
23 *27*, 5982-5987.

24
25 (23) Jian, Z.; Sun, Y.; Ji, X. A new low-voltage plateau of $\text{Na}_3\text{V}_2(\text{PO}_4)_3$ as an anode for Na-ion
26
27 batteries. *Chem. Commun.* **2015**, *51*, 6381-3.

28
29 (24) Wang, Q.; Zhao, B.; Zhang, S.; Gao, X.; Deng, C. Superior sodium intercalation of
30
31 honeycomb-structured hierarchical porous $\text{Na}_3\text{V}_2(\text{PO}_4)_3/\text{C}$ microballs prepared by a facile one-
32
33 pot synthesis. *J. Mater. Chem. A* **2015**, *3*, 7732-7740.

34
35 (25) Jiang, Y.; Yang, Z. Z.; Li, W. H.; Zeng, L. C.; Pan, F. S.; Wang, M.; Wei, X.; Hu, G. T.;
36
37 Gu, L.; Yu, Y. Nanoconfined Carbon-Coated $\text{Na}_3\text{V}_2(\text{PO}_4)_3$ Particles in Mesoporous Carbon
38
39 Enabling Ultralong Cycle Life for Sodium-Ion Batteries. *Adv. Energy Mater.* **2015**, *5*, 1402104.

40
41 (26) Liu, Q.; Meng, X.; Wei, Z.; Wang, D.; Gao, Y.; Wei, Y.; Du, F.; Chen, G. Core/Double-
42
43 Shell Structured $\text{Na}_3\text{V}_2(\text{PO}_4)_2\text{F}_3@\text{C}$ Nanocomposite as the High Power and Long Lifespan
44
45 Cathode for Sodium-Ion Batteries. *ACS Appl. Mater. Interfaces* **2016**, *8*, 31709-31715.

46
47 (27) Rui, X.; Sun, W.; Wu, C.; Yu, Y.; Yan, Q. An Advanced Sodium-Ion Battery Composed
48
49 of Carbon Coated $\text{Na}_3\text{V}_2(\text{PO}_4)_3$ in a Porous Graphene Network. *Adv. Mater.* **2015**, *27*, 6670-6.

50
51 (28) Duan, W. C.; Zhu, Z. Q.; Li, H.; Hu, Z.; Zhang, K.; Cheng, F. Y.; Chen, J. $\text{Na}_3\text{V}_2(\text{PO}_4)_3@\text{C}$
52
53
54
55
56
57
58
59
60

1
2
3
4 core-shell nanocomposites for rechargeable sodium-ion batteries. *J. Mater. Chem. A* **2014**, *2*,
5 8668-8675.

6
7
8
9 (29) Plashnitsa, L. S.; Kobayashi, E.; Noguchi, Y.; Okada, S.; Yamaki, J. Performance of
10 NASICON Symmetric Cell with Ionic Liquid Electrolyte. *J. Electrochem. Soc.* **2010**, *15*,
11 A536-A543.

12
13
14
15 (30) Zhu, C.; Kopold, P.; van Aken, P. A.; Maier, J.; Yu, Y. High Power-High Energy
16 Sodium Battery Based on Threefold Interpenetrating Network. *Adv. Mater.* **2016**, *28*, 2409-
17 16.

18
19
20
21 (31) Shen, W.; Li, H.; Guo, Z.; Wang, C.; Li, Z.; Xu, Q.; Liu, H.; Wang, Y.; Xia, Y. Double-
22 Nanocarbon Synergistically Modified $\text{Na}_3\text{V}_2(\text{PO}_4)_3$: An Advanced Cathode for High-Rate
23 and Long-Life Sodium-Ion Batteries. *ACS Appl. Mater. Interfaces* **2016**, *8*, 15341-51.

24
25
26
27 (32) Ponrouch, A.; Monti, D.; Boschini, A.; Steen, B.; Johansson, P.; Palacín, M. R. Non-
28 aqueous electrolytes for sodium-ion batteries. *J. Mater. Chem. A* **2015**, *3*, 22-42.

29
30
31
32 (33) Hess, S.; Wohlfahrt-Mehrens, M.; Wachtler, M. Flammability of Li-Ion Battery
33 Electrolytes: Flash Point and Self-Extinguishing Time Measurements. *J. Electrochem. Soc.*
34 **2015**, *162*, A3084-A3097.

35
36
37
38 (34) Eshetu, G. G.; Grugeon, S.; Laruelle, S.; Boyanov, S.; Lecocq, A.; Bertrand, J. P.; Marlair,
39 G. In-depth safety-focused analysis of solvents used in electrolytes for large scale lithium ion
40 batteries. *Phys. Chem. Chem. Phys.* **2013**, *15*, 9145-55.

41
42
43
44 (35) Cabrera-Castillo, E.; Niedermeier, F.; Jossen, A. Calculation of the state of safety (SOS)
45 for lithium ion batteries. *J. Power Sources* **2016**, *324*, 509-520.

46
47
48
49 (36) Armand, M.; Endres, F.; MacFarlane, D. R.; Ohno, H.; Scrosati, B. Ionic-liquid materials
50 for the electrochemical challenges of the future. *Nat. Mater.* **2009**, *8*, 621-629.

51
52
53
54 (37) Chancelier, L.; Diallo, A. O.; Santini, C. C.; Marlair, G.; Gutel, T.; Mailley, S.; Len, C.

1
2
3
4 Targeting adequate thermal stability and fire safety in selecting ionic liquid-based electrolytes
5 for energy storage. *Phys. Chem. Chem. Phys.* **2014**, *16*, 1967-1976.

6
7
8
9 (38) MacFarlane, D. R.; Tachikawa, N.; Forsyth, M.; Pringle, J. M.; Howlett, P. C.; Elliott, G.
10 D.; Davis, J. H.; Watanabe, M.; Simon, P.; Angell, C. A. Energy applications of ionic liquids.
11
12
13 *Energ. Environ. Sci.* **2014**, *7*, 232-250.

14
15
16 (39) Watanabe, M.; Thomas, M. L.; Zhang, S.; Ueno, K.; Yasuda, T.; Dokko, K. Application
17 of Ionic Liquids to Energy Storage and Conversion Materials and Devices. *Chem. Rev.* **2017**,
18
19
20
21 *117*, 7190-7239.

22
23 (40) Basile, A.; Hilder, M.; Makhlooghiyazad, F.; Pozo-Gonzalo, C.; MacFarlane, D. R.;
24 Howlett, P. C.; Forsyth, M. Ionic Liquids and Organic Ionic Plastic Crystals: Advanced
25 Electrolytes for Safer High Performance Sodium Energy Storage Technologies. *Adv. Energy*
26
27
28
29
30
31 *Mater.* **2018**, *8*, 1703491.

32 (41) Matsumoto, K.; Okamoto, Y.; Nohira, T.; Hagiwara, R. Thermal and Transport
33 Properties of Na[N(SO₂F)₂]-[N-Methyl-N-propylpyrrolidinium][N(SO₂F)₂] Ionic Liquids for
34 Na Secondary Batteries. *J. Phys. Chem. C* **2015**, *119*, 7648-7655.

35
36
37
38 (42) Forsyth, M.; Yoon, H.; Chen, F.; Zhu, H.; MacFarlane, D. R.; Armand, M.; Howlett, P. C.
39 Novel Na⁺ Ion Diffusion Mechanism in Mixed Organic-Inorganic Ionic Liquid Electrolyte
40 Leading to High Na⁺ Transference Number and Stable, High Rate Electrochemical Cycling of
41 Sodium Cells. *J. Phys. Chem. C* **2016**, *120*, 4276-4286.

42
43
44
45 (43) Wongittharom, N.; Wang, C.-H.; Wang, Y.-C.; Yang, C.-H.; Chang, J.-K. Ionic Liquid
46 Electrolytes with Various Sodium Solutes for Rechargeable Na/NaFePO₄ Batteries Operated
47 at Elevated Temperatures. *ACS Appl. Mater. Interfaces* **2014**, *6*, 17564-17570.

48
49
50
51 (44) Wang, C.-H.; Yang, C.-H.; Chang, J.-K. Suitability of ionic liquid electrolytes for room-
52 temperature sodium-ion battery applications. *Chem. Commun.* **2016**, *52*, 10890-10893.
53
54
55
56
57
58
59
60

- 1
2
3
4 (45) Chagas, L. G.; Buchholz, D.; Wu, L.; Vortmann, B.; Passerini, S. Unexpected performance
5 of layered sodium-ion cathode material in ionic liquid-based electrolyte. *J. Power Sources*
6
7 **2014**, *247*, 377-383.
8
9
10
11 (46) Sui, G.; Jana, S.; Zhong, W. H.; Fuqua, M. A.; Ulven, C. A. Dielectric properties and
12 conductivity of carbon nanofiber/semi-crystalline polymer composites. *Acta Mater.* **2008**, *56*,
13
14 2381-2388.
15
16
17
18 (47) Fang, X.; Ge, M.; Rong, J.; Zhou, C. Free-Standing LiNi_{0.5}Mn_{1.5}O₄/Carbon Nanofiber
19 Network Film as Lightweight and High-Power Cathode for Lithium Ion Batteries. *ACS Nano*
20
21 **2014**, *8*, 4876-4882.
22
23
24
25 (48) Li, W.; Li, M.; Adair, K. R.; Sun, X.; Yu, Y. Carbon nanofiber-based nanostructures for
26 lithium-ion and sodium-ion batteries. *J. Mater. Chem. A* **2017**, *5*, 13882-13906.
27
28
29
30 (49) Matsumoto, K.; Hosokawa, T.; Nohira, T.; Hagiwara, R.; Fukunaga, A.; Numata, K.; Itani,
31 E.; Sakai, S.; Nitta, K.; Inazawa, S. The Na[FSA]-[C₂C₁im][FSA] (C₂C₁im⁺:1-ethyl-3-
32 methylimidazolium and FSA⁻:bis(fluorosulfonyl)amide) ionic liquid electrolytes for sodium
33 secondary batteries. *J. Power Sources* **2014**, *265*, 36-39.
34
35
36
37
38
39 (50) Rodríguez-Carvajal, J. Recent advances in magnetic structure determination by neutron
40 powder diffraction. *Physica B* **1993**, *192*, 55-69.
41
42
43
44 (51) Momma, K.; Izumi, F. VESTA: a three-dimensional visualization system for electronic
45 and structural analysis. *J. Appl. Crystallogr.* **2008**, *41*, 653-658.
46
47
48
49 (52) Brunauer, S.; Emmett, P. H.; Teller, E. Adsorption of Gases in Multimolecular Layers. *J.*
50 *Am. Chem. Soc.* **1938**, *60*, 309-319.
51
52
53
54 (53) Hwang, J.; Matsumoto, K.; Hagiwara, R. Symmetric Cell Electrochemical Impedance
55 Spectroscopy of Na₂FeP₂O₇ Positive Electrode Material in Ionic Liquid Electrolytes. *J. Phys.*
56 *Chem. C* **2018**, *122*, 26857-26864.
57
58
59
60

- 1
2
3
4 (54) Li, H.; Wu, C.; Bai, Y.; Wu, F.; Wang, M. Controllable synthesis of high-rate and long
5 cycle-life $\text{Na}_3\text{V}_2(\text{PO}_4)_3$ for sodium-ion batteries. *J. Power Sources* **2016**, *326*, 14-22.
6
7
8
9
10
11 (55) Jian, Z.; Yuan, C.; Han, W.; Lu, X.; Gu, L.; Xi, X.; Hu, Y.-S.; Li, H.; Chen, W.; Chen,
12 D.; Ikuhara, Y.; Chen, L. Atomic Structure and Kinetics of NASICON $\text{Na}_x\text{V}_2(\text{PO}_4)_3$ Cathode
13 for Sodium-Ion Batteries. *Adv. Funct. Mater.* **2014**, *24*, 4265-4272.
14
15
16 (56) Ferrari, A. C.; Robertson, J. Raman spectroscopy of amorphous, nanostructured,
17 diamond-like carbon, and nanodiamond. *Philos. Trans. Royal Soc. A* **2004**, *362*, 2477-2512.
18
19
20 (57) Ferrari, A. C.; Meyer, J. C.; Scardaci, V.; Casiraghi, C.; Lazzeri, M.; Mauri, F.; Piscanec,
21 S.; Jiang, D.; Novoselov, K. S.; Roth, S.; Geim, A. K. Raman Spectrum of Graphene and
22 Graphene Layers. *Phys. Rev. Lett.* **2006**, *97*, 187401.
23
24
25 (58) Dresselhaus, M. S.; Dresselhaus, G.; Saito, R.; Jorio, A. Raman spectroscopy of carbon
26 nanotubes. *Phys. Rep.* **2005**, *409*, 47-99.
27
28
29 (59) Kaushik S.; Hwang, J.; Matsumoto, K.; Sato, Y.; Hagiwara, R. CuP_2/C Composite
30 Negative Electrodes for Sodium Secondary Batteries Operating at Room-to-Intermediate
31 Temperatures Utilizing Ionic Liquid Electrolyte. *ChemElectroChem* **2018**, *5*, 1340-1344.
32
33
34 (60) Jian, Z. L.; Han, W. Z.; Lu, X.; Yang, H. X.; Hu, Y. S.; Zhou, J.; Zhou, Z. B.; Li, J. Q.;
35 Chen, W.; Chen, D. F.; Chen, L. Q. Superior Electrochemical Performance and Storage
36 Mechanism of $\text{Na}_3\text{V}_2(\text{PO}_4)_3$ Cathode for Room-Temperature Sodium-Ion Batteries. *Adv.*
37 *Energy Mater.* **2013**, *3*, 156-160.
38
39
40 (61) Saravanan, K.; Mason, C. W.; Rudola, A.; Wong, K. H.; Balaya, P. The First Report on
41 Excellent Cycling Stability and Superior Rate Capability of $\text{Na}_3\text{V}_2(\text{PO}_4)_3$ for Sodium Ion
42 Batteries. *Adv. Energy Mater.* **2013**, *3*, 444-450.
43
44
45
46
47
48
49
50
51
52
53
54
55
56
57
58
59
60

- 1
2
3
4 (62) Chen, L.; Zhao, Y.; Liu, S.; Zhao, L. Hard Carbon Wrapped Na₃V₂(PO₄)₃@C Porous
5 Composite Extending Cycling Lifespan for Sodium-Ion Batteries. *ACS Appl. Mater.*
6 *Interfaces* **2017**, *9* (51), 44485-44493.
7
8
9
10 (63) Li, X.; Huang, Y.; Wang, J.; Miao, L.; Li, Y.; Liu, Y.; Qiu, Y.; Fang, C.; Han, J.; Huang,
11 Y. High valence Mo-doped Na₃V₂(PO₄)₃/C as a high rate and stable cycle-life cathode for
12 sodium battery. *J. Mater. Chem. A* **2018**, *6*, 1390-1396
13
14
15 (64) Lim, S.-J.; Han, D.-W.; Nam, D.-H.; Hong, K.-S.; Eom, J.-Y.; Ryu, W.-H.; Kwon, H.-S.
16 Structural enhancement of Na₃V₂(PO₄)₃/C composite cathode materials by pillar ion doping
17 for high power and long cycle life sodium-ion batteries. *J. Mater. Chem. A* **2014**, *2*, 19623-
18 19632.
19
20
21 (65) Ogihara, N.; Itou, Y.; Sasaki, T.; Takeuchi, Y. Impedance Spectroscopy Characterization
22 of Porous Electrodes under Different Electrode Thickness Using a Symmetric Cell for High-
23 Performance Lithium-Ion Batteries. *J. Phys. Chem. C* **2015**, *119*, 4612-4619.
24
25
26 (66) Chen, C. H.; Liu, J.; Amine, K. Symmetric cell approach and impedance spectroscopy of
27 high power lithium-ion batteries. *J. Power Sources* **2001**, *96*, 321-328.
28
29
30 (67) Petibon, R.; Aiken, C. P.; Sinha, N. N.; Burns, J. C.; Ye, H.; VanElzen, C. M.; Jain, G.;
31 Trussler, S.; Dahn, J. R. Study of Electrolyte Additives Using Electrochemical Impedance
32 Spectroscopy on Symmetric Cells. *J. Electrochem. Soc.* **2013**, *160*, A117-A124.
33
34
35 (68) Kang, B.; Ceder, G. Battery materials for ultrafast charging and discharging. *Nature* **2009**,
36 *458*, 190.
37
38
39 (69) Bai, P.; Bazant, M. Z. Charge transfer kinetics at the solid–solid interface in porous
40 electrodes. *Nat. Comm.* **2014**, *5*, 3585.
41
42
43
44
45
46
47
48
49
50
51
52
53
54
55
56
57
58
59
60

1
2
3
4 (70) Cao, Q.; Zhang, H. P.; Wang, G. J.; Xia, Q.; Wu, Y. P.; Wu, H. Q. A novel carbon-
5 coated LiCoO₂ as cathode material for lithium ion battery. *Electrochem. Commun.* **2007**, *9*,
6
7 1228-1232.
8
9
10
11
12
13
14
15
16
17
18
19
20
21
22
23
24
25
26
27
28
29
30
31
32
33
34
35
36
37
38
39
40
41
42
43
44
45
46
47
48
49
50
51
52
53
54
55
56
57
58
59
60